Catalysis Today 173 (2011) 53–61

Contents lists available at ScienceDirect

Catalysis Today

journal homepage: www.elsevier.com/locate/cattod

Selective three-phase hydrogenation of aromatic nitro-compounds over β-molybdenum nitride

Fernando Cárdenas-Lizana[a,*], Daniel Lamey[a], Santiago Gómez-Quero[b], Noémie Perret[c], Lioubov Kiwi-Minsker[a], Mark A. Keane[c]

[a] Group of Catalytic Reaction Engineering, Ecole Polytechnique Fédérale de Lausanne (GGRC-ISIC-EPFL), Lausanne CH-1015, Switzerland
[b] Van't Hoff Institute for Molecular Sciences, University of Amsterdam, Amsterdam 1090 GS, The Netherlands
[c] Chemical Engineering, School of Engineering and Physical Sciences, Heriot-Watt University, Edinburgh EH14 4AS, Scotland, United Kingdom

ARTICLE INFO

Article history:
Received 3 January 2011
Received in revised form 16 March 2011
Accepted 31 March 2011
Available online 12 June 2011

Keywords:
Selective hydrogenation
Liquid phase
Nitroarene
Amine
β-Mo nitride
Hammett relationship

ABSTRACT

A tetragonal molybdenum nitride (β-Mo_2N) has been prepared by temperature programmed treatment of MoO_3 in flowing $N_2 + H_2$ and for the first time shown to catalyze the liquid phase selective hydrogenation (T = 423 K; P_{H_2} = 11 bar) of a series of *para*-substituted (–H, –OH, –O–CH_3, –CH_3, –Cl, –I and –NO_2) nitrobenzenes to give the corresponding aromatic amine. Reaction over Pd/Al_2O_3, as a benchmark catalyst (Pd particle size *ca.* 18 nm), resulted in a composite hydrodechlorination/hydrogenation of *p*-chloronitrobenzene (as a representative nitroarene) to generate nitrobenzene and aniline. β-Mo_2N has been characterized in terms of temperature-programmed reduction (TPR), H_2 chemisorption/temperature programmed desorption (TPD), BET surface area/pore volume, elemental analysis, powder X-ray diffraction (XRD), X-ray photoelectron spectroscopy (XPS), scanning (SEM) and transmission (TEM) electronic microscopy. Elemental analysis, XRD, SEM and TEM have confirmed the formation of tetragonal β-Mo_2N, characterized by an agglomeration of flake-like crystallites. *Post*-synthesis, the nitride was passivated by contact with 1% (v/v) O_2/He at ambient temperature and XPS analysis has demonstrated the formation of a superficial passivating oxide overlayer without bulk oxidation. *Pre*-reaction, activation by TPR to 673 K was necessary to remove the passivating film. Hydrogen TPD has revealed significant hydrogen uptake (0.7 μmol m^{-2}) associated with β-Mo_2N. Nitro group reduction kinetics have been subjected to a Hammett treatment where the reaction constant (ρ = 0 4) is diagnostic of an increase in rate due to the presence of electron-withdrawing substituents on the aromatic ring, consistent with a nucleophilic mechanism. The results presented in this study establish the viability of β-Mo_2N to promote selective nitroarene hydrogenation.

1. Introduction

Aromatic amines are used extensively as intermediates in the manufacture of fine chemicals, pharmaceutical and agricultural products [1]. Standard synthesis routes based on Fe-promoted reduction in acid media (Béchamp reaction) do not meet the current requirements for sustainable process design due to low selectivity to the target amine and the production of large quantities of toxic waste [2]. The alternative catalytic approach *via* batch liquid phase hydrogenation using conventional transition metal (*e.g.* Ni and Pd) catalysts shows promise in terms of increased conversion [3–5] but the low overall reaction selectivity represents a drawback that must be addressed [6]. Taking the hydrogenation of *p*-chloronitrobenzene (*p*-CNB) to *p*-chloroaniline (*p*-CAN), undesirable C–Cl hydrogenolysis is difficult to circumvent at high conversions [2]. Indeed, Mo et al. [7] and Li and co-workers [8] have recently reported the formation of nitrobenzene (NB) and aniline (AN) in the hydrogenation of *p*-CNB over unsupported NiB nanotubes and nanospheres. Low selectivity with respect to –NO_2 group reduction also extends to gas phase operation where cyclohexylamine and NB have been identified as secondary products in the hydrotreatment of NB and *o*-CNB over polymer-supported Pt [9] and Pd/Al_2O_3 [10], respectively. Application of coupling reactions [11], support modifications (*e.g.* polymer functionalisation [12], carbon nanofibre orientation [13], magnetization of γ-Al_2O_3 [14]) and/or the use of bi- (Ni–B [5], NiPB [15] or Pt–Pd [16]) and tri- (NiCoB [17]) metallic systems have been examined as a possible means of enhancing selectivity. However, the associated complexity and costs militate against the viability of these approaches in terms of process scale up. There is now a pressing need for a more efficient catalyst system to promote the selective hydrogenation of aromatic polyfunctional nitroarenes.

* Corresponding author. Tel.: +41 021 693 31 86.
E-mail address: fernando.cardenaslizana@epfl.ch (F. Cárdenas-Lizana).

0920-5861/$ – see front matter © 2011 Elsevier B.V. All rights reserved.
doi:10.1016/j.cattod.2011.03.084

Nomenclature

AAS	absorption atomic spectroscopy
AN	aniline
BE	binding energy (eV)
BET	BET surface area ($m^2\,g^{-1}$).
C_i	concentration of compound *i* in bulk liquid ($mol\,dm^{-3}$)
p-CNB	*para*-chloronitrobenzene
p-CAN	*para*-chloroaniline
d_{chem}	Pd particle size from hydrogen chemisorption measurements (nm)
d_i	diameter of the *i*th Pd metal particle (nm)
d_{TEM}	mean Pd particle size from TEM analysis (nm)
GHSV	gas hourly space velocity
$M_{p\text{-CNB}}$	*p*-CNB molar mass
n_i	number of Pd metal particles with diameter d_i
NB	nitrobenzene
o-CNB	*ortho*-chloronitrobenzene
P_{H_2}	hydrogen partial pressure (bar)
R_i	initial hydrogenation rate of the *para*-substituted nitroarene ($mol\,dm^{-3}\,min^{-1}$)
R_0	initial NB hydrogenation rate ($mol\,dm^{-3}\,min^{-1}$)
S_i	selectivity with respect to compound *i*
SEM	scanning electron microscopy
S_{Pd}	specific Pd surface area ($m^2_{Pd}\,g^{-1}_{Pd}$)
T	temperature (K)
t	time (min)
TCD	thermal conductivity detector
TEM	transmission electron microscopy
TPD	temperature programmed desorption
TPR	temperature programmed reduction
x_i	molar fraction of compound *i*
X_i	conversion of reactant *i*
XPS	X-ray photoelectron spectroscopy
XRD	X-ray diffractometry

Greek letters

ρ	Hammett reaction constant
$\rho_{p\text{-CNB}}$	density of *p*-CNB ($g\,cm^{-3}$)
ρ_{Pd}	density of Pd ($g\,cm^{-3}$)
σ_i	Hammett substituent constant

The use of molybdenum nitrides in hydrogen mediated reactions is attracting increasing attention as a viable alternative to conventional transition metal catalysts. Li et al. [18], studying the hydrogenation of long chain alkadienes over Mo nitrides, reported an up to 54% increase in conversion (relative to Pd/Al_2O_3) and enhanced selectivity to an alkene product that was governed by the Mo^0/Mo^{m+} ($m = 2,3$) ratio. Hydrogenation activity of molybdenum nitrides can be linked to a modification of electronic density and contraction of the *d*-band due to the interstitial introduction of nitrogen in the Mo lattice [19], resulting in an increased capacity for H_2 adsorption [20]. Mo nitrides have now been successfully used to promote NO reduction [21,22] and the hydrogenation of CO [23] and ethyne [24]. The potential for Mo_2N application in the selective hydrogenation of polyfunctional reactants has also been flagged [25]. Guerrero-Ruiz et al. [26] reported high selectivites to the less thermodynamically favoured crotyl alcohol (from crotonaldehyde) over mesorporous carbon supported Mo nitride and correlated this to a preferential activation of the C=O group on the (2 0 0) plane. Taking the possible allotropic forms, cubic γ-Mo_2N has been the more widely studied [21–26] in terms of hydrogen mediated catalytic applications. However, Mckay et al. [27] have reported a higher catalytic activity for (tetragonal) β-Mo_2N when compared with δ-MoN and γ-Mo_2N in ammonia synthesis. A comprehensive search through the literature failed to unearth any instance where Mo nitride has been used in the liquid phase catalytic hydrogenation of nitroarenes. We have recently reported [28] results for the gas phase hydrogenation of *p*-CNB over β-Mo_2N, where we recorded reaction exclusivity in terms of *p*-CAN as (the only) product. We have now extended that work and consider herein the application of β-Mo_2N to catalyze the liquid phase hydrogenation of *p*-CNB, where catalytic performance is assessed against a standard Pd/Al_2O_3 catalyst. Furthermore, the catalytic action of β-Mo_2N to promote $-NO_2$ group reduction for a series or *para*-substituted nitroarenes has been investigated and the catalytic data have been subjected to a Hammett treatment.

2. Experimental

2.1. Materials and analytical methods

The reactants (NB, *p*-nitrophenol, *p*-nitroanisole, *p*-nitrotoluene, *p*-CNB, *p*-iodonitrobenzene and *p*-dinitrobenzene, Sigma–Aldrich ≥98%) and solvent (ethanol, Sigma–Aldrich ≥99%) were used as supplied, without further purification. All the gases used in this study (H_2, N_2, Ar, O_2 and He) were of ultra high purity (>99.99%, Carbagas). The composition of the reaction/product mixtures was determined using a Perkin-Elmer Auto System XL chromatograph equipped with a programmed split/splitless injector and a flame ionization detector, employing a Stabilwax (Cross-bond Carbowax-PEG, Restek, USA) capillary column (*i.d.* = 0.32 mm, length = 30 m, film thickness = 0.25 μm). Data acquisition and manipulation were performed using the TotalChrom Workstation (Version 6.3.2 for Windows) chromatography data system. Reactant and product molar fractions (x_i) were obtained using detailed calibration plots (not shown) where the total mass balance in the mixture (based on GC analysis) was analyzed for every extracted sample. The extent of hydrogenation can be represented by the reactant fractional conversion where, taking *p*-CNB ($X_{p\text{-CNB}}$) as representative reactant

$$X_{p\text{-CNB}} = 1 - x_{p\text{-CNB}} \quad (1)$$

and selectivity in terms of *p*-CAN ($S_{p\text{-CAN}}$) as target product is given by(2)$S_{p\text{-CAN}} = x_{p\text{-CAN}} / \sum_{\text{products}} x_i$The concentration of organic species in the bulk liquid phase (C_i, $mol\,dm^{-3}$) was determined assuming that the density was constant and equal to that of *p*-CNB ($\rho_{p\text{-CNB}} = 1.298\,g\,cm^{-3}$) [29]

$$C_i = x_i \times \left(\frac{\rho_{p-\text{CNB}}}{M_{p-\text{CNB}}} \right) \quad (3)$$

and $M_{p\text{-CNB}}$ represents *p*-CNB molar mass.

2.2. Catalyst preparation

2.2.1. β-Mo_2N

Mo nitride synthesis was conducted in a horizontally mounted quartz reactor *via* the temperature programmed reduction–nitridation of MoO_3 (99.9995%, Alfa Aesar) in a continuous flow of $H_2 + N_2$ at atmospheric pressure. The precursor (*ca.* 4 g MoO_3) was loaded into the tubular reactor (30 cm × 1 cm *i.d.*) and heated in 30 $cm^3\,min^{-1}$ (*GHSV* = 460 h^{-1}, Bronkhorst mass flow controlled) 15% (v/v) N_2/H_2 at 5 K min^{-1} to 933 K, maintaining the final temperature for 100 h. The reaction was quenched by switching to an Ar flow (30 $cm^3\,min^{-1}$) for 1 h and cooling to room temperature. Samples for off-line analysis were passivated (at 293 K) in 1% (v/v) O_2/He; there was no detectable temperature

increase during sample passivation. The latter step was introduced to avoid uncontrolled sample oxidation upon exposure to air [30]. Prior to use, the nitride was activated in 60 $cm^3\ min^{-1}$ H_2 at 2 K min^{-1} to 673 K and maintained at the final isothermal hold for 1 h.

2.2.2. Pd/Al_2O_3

The Al_2O_3 support was obtained from Sigma–Aldrich and used as received. Five Pd supported samples (0.1, 0.5, 1, 2 and 4% wt.) were synthesized by deposition of *ex-situ* prepared monodispersed Pd^0 nano-particles. An aqueous solution of $PdCl_2$ (Fluka, >99%) and $Na_2MoO_4{\cdot}H_2O$ (Fluka, >99%) (Pd/Mo mol ratio = 1) was heated at *ca.* 368 K (under continuous stirring) until complete evaporation. The solid residue was dissolved in water and contacted (at room temperature) with a continuous flow of H_2 (100 $cm^3\ min^{-1}$) for 30 min. This procedure has been demonstrated [31] to result in the formation of uniform Pd^0 nano-particles stabilized by molybdate anions. Pd nano-particle deposition was achieved *via* adsorption where the Al_2O_3 support (*ca.* 2 g) was immersed in a stirred aqueous solution (*ca.* 500 cm^3) containing the target Pd loading until the solution was colourless (*ca.* 2 h), *i.e.* complete deposition. The slurry was then filtered, dried in air at room temperature and sieved into a batch of 75 μm average diameter. Prior to use, the catalyst was activated in 60 $cm^3\ min^{-1}$ H_2 at 2 K min^{-1} to 493 K and maintained at the final isothermal hold for 1 h.

2.2.3. Catalyst characterization

Nitride elemental (nitrogen) analysis was determined using an Exeter CE-440 Elemental Analyser after sample combustion at *ca.* 1873 K. The Pd content (in Pd/Al_2O_3) was measured by absorption atomic spectroscopy (AAS) using a Shimadzu AA-6650 spectrometer with an air-acetylene flame from the diluted extract in aqua regia (25%, v/v HNO_3/HCl). Temperature programmed reduction (TPR), H_2 chemisorption, temperature programmed desorption (TPD) and BET surface areas were obtained using the CHEM-BET 3000 unit. The characterization measurements were carried out *in situ* following the reduction/nitridation/passivation steps. TPR analysis was conducted by heating the sample in 17 $cm^3\ min^{-1}$ 5% (v/v) H_2/N_2 at 2 K min^{-1} to 673 K (β-Mo_2N) or 493 K (Pd/Al_2O_3). The exit gas passed through a liquid N_2 trap and changes in H_2 consumption/release were monitored by TCD with data acquisition/manipulation using the TPR Win™ software. The reduced samples were maintained at the final temperature until the signal returned to baseline. The samples were then swept with 65 $cm^3\ min^{-1}$ N_2 for 1.5 h, cooled to room temperature and subjected to H_2 chemisorption using a pulse (10 μl) titration procedure. Hydrogen TPD was conducted in a N_2 flow (65 $cm^3\ min^{-1}$) at 50 K min^{-1} to 873 K. BET areas were recorded with a 30% (v/v) N_2/He flow using pure N_2 as internal standard. At least two cycles of N_2 adsorption–desorption in the flow mode were employed to determine total surface area using the standard single point method. Pore volume measurements were performed using the commercial Micromeritics Flowsorb II 2300 unit. Prior to analysis, the samples were outgassed at 423 K for 1 h and the total pore volume was obtained at a relative N_2 pressure (P/P_0) = 0.95. BET surface area, pore volume and H_2 consumption/release measurements were reproducible to within ±5%; the values quoted represent the mean.

Powder X-ray diffractograms (XRD) were recorded on a Bruker/Siemens D500 incident X-ray diffractometer using Cu Kα radiation. The samples were scanned at a rate of 0.02° $step^{-1}$ over the range $20° \le 2\theta \le 90°$ (scan time = 5 s $step^{-1}$). Diffractograms were identified using the JCPDS-ICDD reference standard, *i.e.* β-Mo_2N (25-1368), Pd (46-1043) and δ-Al_2O_3 (47-1770). Lattice parameters were determined by means of the CELLREF software and used to determine the crystal structure of the β-Mo_2N using the CrystalMaker software. X-ray photoelectron spectroscopy (XPS) analyses were conducted on an Axis Ultra instrument (Kratos) using a monochromatic Al Kα X-ray source (1486.6 eV). Prior to analysis, the nitride sample was adhered to a conducting carbon tape, mounted in the sample holder and subjected to ultra-high vacuum conditions (<10^{-8} Torr). The source power was maintained at 150 W and the emitted photoelectrons were sampled from a square area of 750 μm × 350 μm; the photoelectron take-off angle was 90°. The analyzer pass energy was 80 eV for survey spectra (0–1000 eV) and 40 eV for high resolution spectra (over the Mo $3d_{3/2}$ and Mo $3d_{5/2}$ binding energy (BE) range, 227–239 eV). The adventitious C 1s peak was calibrated at 284.5 eV and used as internal standard to compensate for any charging effects. Spectral curve fitting and quantification employed the CasaXPS software, using relative sensitivity factors provided by Kratos.

Analysis by scanning electron microscopy (SEM) was conducted using a Philips FEI XL30-FEG equipped with an Everhart-Thornley secondary-electron detector operated at an accelerating voltage of 10–15 kV and a NORAN System SIX (version 1.6) for data analysis. The samples were subjected to a hydrocarbon decontamination treatment using a plasma-cleaner (EVACTRON). Transmission electron microscopy measurements were performed using a JEOL JEM 2011 HRTEM unit with a UTW energy dispersive X-ray detector (Oxford Instruments) operated at an accelerating voltage of 200 kV using Gatan DigitalMicrograph 3.4 for data treatment. The specimens were prepared by dispersion in acetone and deposited on a holey carbon/Cu grid (300 Mesh). Up to 400 individual Pd metal particles were counted for each catalyst and the mean metal diameter (d_{TEM}) was calculated from:

$$d_{TEM} = \frac{\sum_i n_i d_i}{\sum_i n_i} \quad (4)$$

where n_i is the number of particles of diameter d_i. The size limit for the detection of Pd particles is *ca.* 1 nm.

2.3. Catalytic system

Liquid phase hydrogenation reactions (T = 423 K; $P_{H_2} = 11$ bar) were carried out in a commercial semi-batch stirred stainless steel reactor (100 cm^3 autoclave, Büchi AG, Uster, Switzerland) equipped with a pressure controlled H_2 supply system. Madon and Boudart demonstrated [32] that, for heterogeneous catalytic systems operating with negligible mass transfer limitations, a proportional correlation between activity and the number of active sites can be established for a series of catalysts with different metal content but similar dispersion, *i.e.* invariant specific activity. Taking this approach, the (0.1–4% wt.) Pd/Al_2O_3 catalysts were used to determine working conditions where the reaction proceeded under kinetic control. The associated linear relationships (not shown) established reactor operation in the absence of mass transfer constraints for hydrogenation rates < 72×10^5 $\mu mol_{-NO_2}\ mol^{-1}\ min^{-1}$. Detailed testing to determine the activity/selectivity response employed 1% wt Pd/Al_2O_3 as a representative catalyst. Hydrogen consumption in the reactor vessel was monitored on-line with a press flow gas controller (BPC-6002, Büchi, Switzerland) and a stainless steel 6-blade disk turbine impeller (equipped with a self-gassing hollow shaft) provided effective agitation at 1800 rpm. A recirculator (HAAKE B-N3) was used to stabilize the reaction temperature to within ±1 K using oil (Shell Thermia; thermal conductivity = 0.45 kJ $m^{-1}\ h^{-1}\ K^{-1}$; specific heat = 2.4 kJ $kg^{-1}\ K^{-1}$) as the thermal medium. At the beginning of each experiment, a 60 cm^3 ethanolic solution of the nitroarene reactant was charged and flushed three times with N_2 under constant agitation. The catalyst was activated *ex-situ* in a quartz reactor (300 mm length; *i.d.* = 10 mm; 60 $cm^3\ min^{-1}$ H_2; *GHSV* = 200 h^{-1}) to

Table 1
Nitrogen content, Pd loading, BET surface area, total pore volume, characteristic temperature programmed reduction (TPR) T_{max} with associated H_2 consumption, H_2 uptake/TPD measurements, Pd particle size range and mean (d_{TEM}) and XPS binding energies associated with β-Mo_2N.

	β-Mo_2N	Pd/Al_2O_3
Nitrogen content (%, w/w)[a]	5	–
Pd loading (%, w/w)[b]	–	0.92
BET ($m^2\,g^{-1}$)	7[c] (3)[d]	157
Pore volume ($cm^3\,g^{-1}$)	0.02	0.2
TPR T_{max} (K)	637	332
H_2 consumed ($\mu mol\,g^{-1}$)	303	–
H_2 chemisorption ($\mu mol\,g^{-1}$)	0.29	3.9
TPD T_{max} (K)	750, 806, 900	–
H_2 desorbed ($\mu mol\,m^{-2}$)	0.7	–
Pd size range (nm)	–	3–30
d_{TEM} (nm)	–	18
XPS Mo $3d_{5/2}$ BE (eV)	228.5, 233.0	–

[a] From elemental analysis.
[b] From AAS.
[c] Activated nitride.
[d] Passivated nitride.

493 K (Pd/Al_2O_3) or 673 K (β-Mo_2N) at 2 K min^{-1}, cooled to room temperature and kept in an inert (N_2) atmosphere. The catalyst was then fluidized in a flow of N_2, transferred to the reactor and the temperature was stabilized (*ca.* 45 min) under gentle stirring (*ca.* 300 rpm). Hydrogen was then introduced, the system was pressurized (to 20 ± 0.5 bar, up to 20 times in excess of the stoichiometric requirements for hydrogenation to the respective amine) and stirring (at 1800 rpm) was engaged (time $t = 0$ for reaction). In a series of blank tests, reactions carried out in the absence of catalyst did not result in any measurable conversion. The initial $-NO_2/Mo_2N$ (or Pd) molar ratio spanned the range 0.2–480. A *non*-invasive liquid sampling system *via* a syringe with in-line filters allowed a controlled removal of aliquots (≤0.5 cm^3) from the reactor. Repeated reaction runs with the same batch of catalyst delivered conversion/selectivity values that were reproducible to within ±5%.

3. Results and discussion

3.1. Catalyst characterization

3.1.1. β-Mo_2N

3.1.1.1. BET area-pore volume/XPS/TPR. The BET area associated with the *as prepared* nitride (7 $m^2\,g^{-1}$, see Table 1) is close to that reported in the literature (9 $m^2\,g^{-1}$) [33] for β-Mo_2N synthesized *via* temperature programmed treatment of MoO_3 in N_2/H_2. We could not find any published pore volume data with which to compare our measurement (0.02 $cm^3\,g^{-1}$). β-Mo_2N passivation was conducted in a flow of diluted (1%, v/v) O_2 (see Section 2) to generate a protective oxide film on the nitride surface and circumvent bulk oxidation [34]. This passivation layer has been characterized as chemisorbed oxygen associated with Mo surface atoms [35,36]. XPS analysis was conducted to characterize the passivated nitride surface and the spectra over the Mo 3*d* (Mo $3d_{3/2}$ and $3d_{5/2}$) BE region for the MoO_3 precursor (A) and passivated β-Mo_2N (B) can be compared in Fig. 1; the associated BE values are given in Table 1. The XPS profile for MoO_3 exhibits a single spin-orbit doublet (Mo $3d_{5/2}$:$3d_{3/2}$ = 3:2, Mo atom % = 27, O atom % = 73) with a Mo $3d_{5/2}$ BE = 233.0 eV that is characteristic of Mo^{6+} [37,38]. The XPS profile for the passivated β-Mo_2N (Fig. 1(B)) shows a second predominant doublet at a lower binding energy (Mo $3d_{5/2}$ = 228.5 eV). While the XPS peaks for Mo^{6+} in MoO_3 are strong and well defined, they are noticeably less intense in the passivated β-Mo_2N and the strong signal at lower BE can be associated with nitride character (lower Mo oxidation state). Li et al. [18] using an advanced deconvolution to resolve a single Mo $3d_{5/2}$ signal for the XPS analysis of Mo nitrides and carbides reported a range of Mo^{m+} oxidation states (*m* varying from 0 to 6) assigned to BE values in the range 227.8–233.1 eV. Mckay et al. [39], in their XPS analysis of passivated Mo_2N films on ZSM-5, also recorded a residual Mo^{6+} doublet (Mo $3d_{5/2}$ at 233.0 eV) that they attributed to the passivating oxide layer, which was readily removed by brief Ar ion etching. *Post*-passivation, there was a measurable decrease in BET (from 7 to 3 $m^2\,g^{-1}$), as observed elsewhere [40]. Choi et al. [41] have suggested that a reduction in surface area is the result of O_2 dissolution in Mo_2N. The removal of the passivating layer was investigated by TPR and the result is presented in Fig. 2(A). The TPR profile exhibits a broad positive (hydrogen consumption) peak with T_{max} = 637 K, which can be ascribed to the reduction of the surface oxide layer with water release [35]. It should be noted that higher temperatures (by up to 400 K) are required for MoO_3 reduction [42], consistent with a more facile removal of the superficial passivating layer. Gong and co-workers [33] observed a single reduction peak (at 700 K) during the TPR of passivated β-Mo_2N while Colling et al. [36] reported the desorption of H_2O associated with the reduction of the passivated surface of γ-Mo_2N at $T > 400$ K. As the TPR signal returned to baseline in the isothermal hold (see Fig. 2(A)), a final temperature of 673 K was deemed to be sufficient for β-Mo_2N activation.

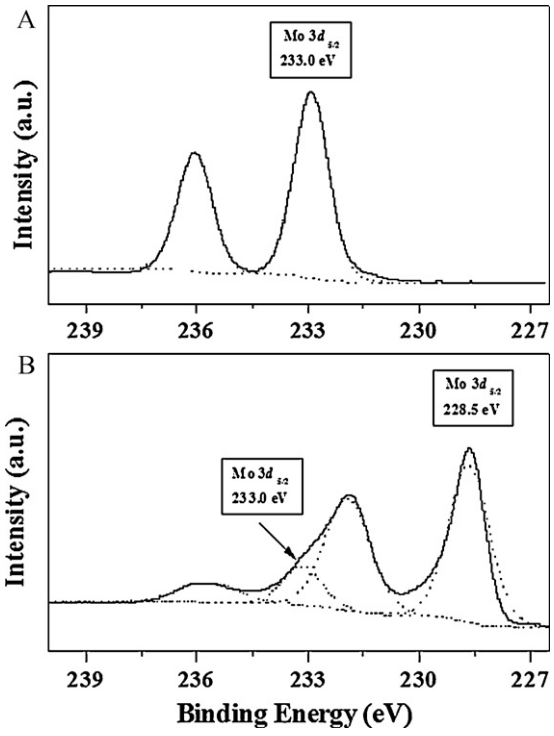

Fig. 1. XPS spectra in the Mo 3*d* region of (A) MoO_3 and (B) passivated β-Mo_2N. *Note*: Experimental values are represented by solid lines and dotted lines illustrate peak deconvolution from curve fitting analysis.

3.1.1.2. Elemental analysis/XRD/TEM/SEM. The bulk nitrogen content for β-Mo_2N obtained from elemental analysis (5%, w/w) was close to the surface content (*ca.* 8%, w/w) obtained by XPS and is in accordance with reported values [33,34]. The XRD pattern of the passivated nitride (Fig. 3(A)) corresponds to the β-Mo_2N reference (JCPDS-ICDD, 25-1368) with reflections at 37.7°, 43.1°, 45.3°, 62.7°, 64.3°, 75.5°, 78.6° and 80.5° associated with the (1 1 2), (2 0 0), (0 0 4), (2 2 0), (2 0 4), (3 1 2), (1 1 6) and (2 2 4) planes. There was no evidence of any bulk oxide (MoO_3 or MoO_2), confirming that the oxide precursor had been completely converted to the nitride where the passivation procedure resulted in a superficial (as opposed to bulk) oxidation as indicated by the XPS measurements.

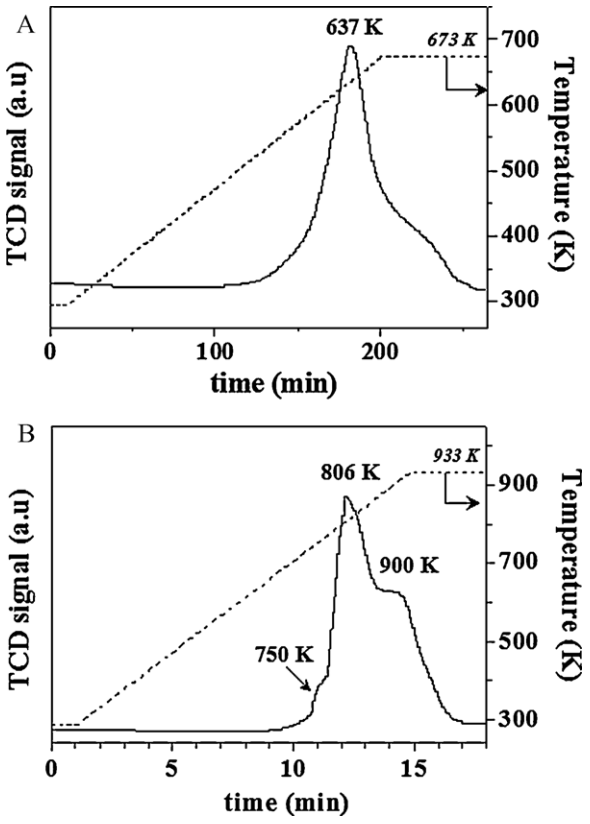

Fig. 2. (A) TPR profile for passivated β-Mo_2N and (B) TPD from activated β-Mo_2N.

While the XRD results are consistent with β-Mo_2N synthesis, the characteristic diffraction peaks for the β-form are very close to those of the γ-allotrope. In order to check for a possible γ-nitride content, the passivated nitride was subjected to a single crystal analysis using the CELLREF software for lattice parameter optimization. The results are given in Table 2, where the residual error when adjusting the *d*-spacing to tetragonal β-Mo_2N is up to 50 times lower than that for cubic γ-Mo_2N. Indeed, the results actually show a better adjustment to β-Mo_2N for the passivated sample relative to the JCPDS-ICDD standard (25-1368). The crystal structure of the tetragonal β-Mo_2N unit cell obtained from the lattice parameters extracted by simulation with CELLREF is shown as an inset in Fig. 3(A), where the atomic arrangement has been established following Ettmayer's approach [43]. A representative high resolution TEM image is presented in Fig. 3(B), where the associated diffractogram pattern has been included as an inset. The *d*-spacings (0.24, 0.21 and 0.20 nm) between the planes in the atomic lattice match, respectively, the (1 1 2), (2 0 0) and (0 0 4) planes of β-Mo_2N. Morphological features were assessed by SEM analysis and the results are presented in Fig. 3(C). The micrograph reveals an agglomeration of flake-like ensembles in the micron range (*ca.* 1–5 μm; see enlarged image in the inset). A similar structure has been reported elsewhere for β-Mo_2N [27,44] and associated with water release during the reduction of MoO_3, which precedes the nitridation step. This results in a significant disruption to the platelet orthorhombic crystal structure that characterizes the starting MoO_3, *i.e.* a *non*-topotactic transformation [28]. This differs from published findings [45,46] where the platelet morphology was maintained.

Table 2
Lattice parameters and residual error associated with the main planes for γ-Mo_2N and β-Mo_2N obtained from the JCPDS-ICDD reference and the Mo nitride synthesized in this work.

Cubic γ-Mo_2N			Tetragonal β-Mo_2N		
h k l	Residual error (%)		*h k l*	Residual error (%)	
	25-1366[a]	This work		25-1368[a]	This work
1 1 1	0.09	0.18	1 1 2	0.13	0.01
2 0 0	0.06	0.47	2 0 0	0.10	0.02
2 2 0	0.08	0.54	0 0 4	0.05	0.02
3 1 1	0.17	0.40	2 2 0	0.03	0.04
2 2 2	0.09	0.15	2 0 4	0.02	0.03
			3 1 2	0.08	0.01
			1 1 6	0.01	0.02
			2 2 4	0.08	0.03
Lattice parameters	*a* = 4.168	*a* = 4.144		*a* = 4.192	*a* = 4.196
				c = 8.039	*c* = 8.008

[a] JCPDS-ICDD standard reference.

3.1.1.3. Hydrogen chemisorption/TPD. *Post*-TPR, β-Mo_2N exhibited a measurable ambient temperature H_2 uptake (0.29 μmol g^{-1}, Table 1). We were unable to find any comparable measurement of H_2 chemisorption on β-Mo_2N in the literature. We should, however, flag the work of Li et al. [47] who demonstrated room temperature hydrogen adsorption on Mo_2N, although the crystallographic phase was not identified. In addition, Saito and Anderson [48] recorded an uptake of 14.3 μmol g^{-1} on γ-Mo_2N + Mo (BET = 7.3 m^2 g^{-1}). The dynamics of H_2 adsorption on group VI metal nitrides is still not well understood. Furimsky in his review [20] has considered H_2 activation on nitrogen deficient Mo–N sites, which leads to a heterolytic interaction with possible dissociative adsorption. The limited published work suggests that H_2 chemisorption capacity is dependent on temperature [49] and nitride surface area [50]. Li et al. [51], studying H_2 adsorption on β-Mo_2N, recorded an order of magnitude greater uptake (from 12 to 173 μmol g^{-1}) with increasing temperature (308 K → 623 K) that

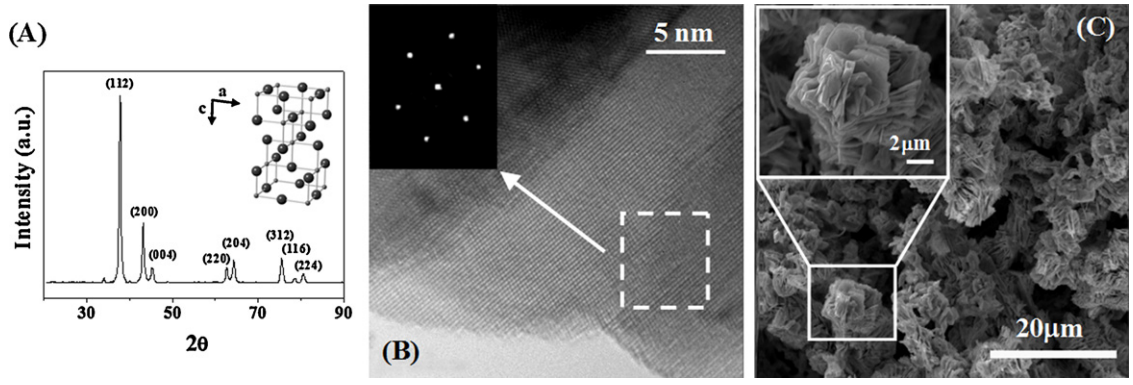

Fig. 3. (A) XRD pattern with tetragonal crystal unit cell, (B) representative TEM image (with diffractogram pattern) and (C) SEM micrograph (with magnified image as inset) of β-Mo_2N. *Note*: XRD peak/plane assignments are based on JCPDS-ICDD standard for β-Mo_2N (25-1368).

they attributed to the formation of a stable hydride phase in the nitride sub-surface. Temperature programmed desorption analysis, subsequent to H_2 chemisorption, demonstrated a significant quantity of H_2 associated with β-Mo_2N (see Fig. 2(B) and Table 1) where the amount desorbed was appreciably greater (by up to a factor of 20) than that measured by chemisorption and must result from hydrogen uptake during TPR. The total H_2 desorbed ($0.7\ \mu mol\ m^{-2}$) is close to that reported ($0.8\ \mu mol\ m^{-2}$) by Li and co-workers [51]. The TPD profile presents a broad peak, extending from *ca.* 700 K into the final isothermal hold (933 K) with a T_{max} at 806 K and two shoulders at 750 K and 900 K. This response suggests the release of a hydrogen component that interacts to varying degrees with β-Mo_2N. The possibility of strongly bound hydrogen species in the sub-layers and/or bulk Mo_2N has been proposed [47]. Choi et al. [52] observed a high temperature peak (at *ca.* 800 K) for H_2 TPD from a β-$Mo_{16}N_7$ thin film and associated this with hydrogen desorption from high energy sub-surface sites. Li et al. [47] demonstrated that hydrogen adsorbed at room temperature desorbed in the temperature range 600–773 K and suggested a surface dissociative adsorption on Mo–N pairs with migration from low to high energy sites. Moreover, Haddix and co-workers [53], using NMR to probe hydrogen interaction with Mo_2N, concluded that strongly bound hydrogen atoms can be generated at room temperature, occupying *ca.* 10% of the total (BET) surface area, suggesting adsorption at nitrogen deficient sites on the surface. A depletion in nitrogen content has been suggested for thermal treatments ($T > 823$ K) [35,36,52]. There was no detectable (by XRD) alteration to nitride structure resulting from the TPD measurements in this study and no significant change in nitrogen content (from elemental analysis).

3.1.2. Pd/Al_2O_3

A 1% (w/w) Pd/Al_2O_3 was chosen as a reference catalyst against which the catalytic performance of β-Mo_2N was assessed; critical structural characteristics are given in Table 1. The BET area ($157\ m^2\ g^{-1}$) is within the range ($75–178\ m^2\ g^{-1}$) of values reported in the literature for δ-Al_2O_3 [54,55]. The recorded TPR profile is shown in Fig. 4(A) and presents a single sharp negative peak (H_2 release) at 332 K, which can be ascribed to the decomposition of Pd hydride formed by H_2 absorption where $P_{H_2} > 0.013$ atm [56]. Hydride composition (H/Pd molar ratio) is dependent on Pd particle size where an increase in Pd dispersion is accompanied by a concomitant enhancement in surface-to-bulk atom ratio with a decrease in the void space available for H_2 diffusion in the metal cluster [57]. The value recorded in this study ($= 0.31\ \mu mol_H\ \mu mol_{Pd}^{-1}$) is significantly lower than that reported [58,59] for bulk Pd ($0.66–0.73\ \mu mol_H\ \mu mol_{Pd}^{-1}$), suggesting the presence of a well dispersed Pd phase. There was no evidence of any H_2 consumption prior to hydride decomposition, confirming the presence of Pd^0 in the *as-prepared* sample (see Section 2.2.2). Hydrogen chemisorption was an order of magnitude greater than that recorded for β-Mo_2N (see Table 1) and close to the value reported ($0.3\ mmol\ g_{Pd}^{-1}$) elsewhere [60] for Pd/Al_2O_3 prepared by standard impregnation ($d_{TEM} = 20$ nm), suggesting a similar metal dispersion to the catalyst used in this study. Indeed, a Pd particle size of *ca.* 14 nm was calculated from H_2 chemisorption ($d_{chem} = 6/(S_{Pd} \times \rho_{Pd})$ where $\rho_{Pd} = 12.02\ g_{Pd}\ cm_{Pd}^{-3}$), assuming spherical morphology [57,61] and exclusive dissociative adsorption (H_2:Pd = 1:2) [62,63]. XRD analysis generated the diffractogram shown in Fig. 4(B), which is dominated by a peak at *ca.* 67° due to the (4 4 2) plane of δ-Al_2O_3. In addition to the support peaks, there are reflections due to a Pd metal phase, *i.e.* at $2\theta = 40.1°$, 46.7° and 82.1° corresponding to (1 1 1), (2 0 0) and (3 1 1) planes, respectively. The representative TEM micrograph shown in Fig. 4(C) demonstrates that Pd is present as discrete particles (≤30 nm) with a mean size

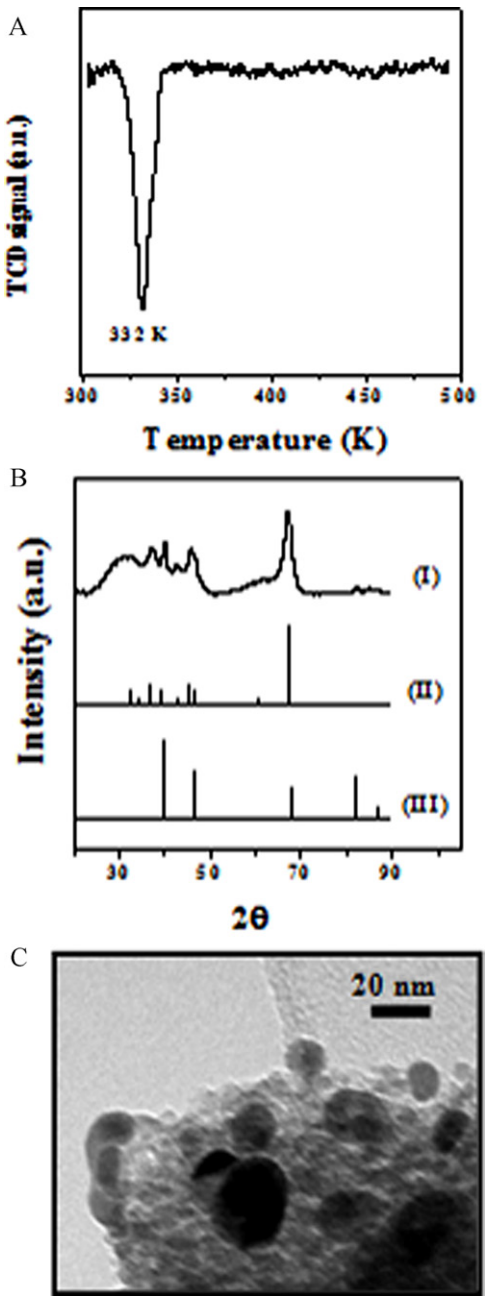

Fig. 4. (A) TPR profile for Pd/Al_2O_3; (B) XRD diffractograms for (I) activated Pd/Al_2O_3 and JCPDS-ICDD reference for (II) δ-Al_2O_3 (47-1770) and (III) Pd (46-1043); (C) representative TEM image of Pd/Al_2O_3.

of 18 nm (Table 1) that is consistent with the H_2 chemisorption measurement.

3.2. Catalyst activity/selectivity

3.2.1. Hydrogenation of p-chloronitrobenzene

The observed capacity of β-Mo_2N for hydrogen uptake/desorption (Table 1) suggests a catalytic hydrogenation capability that was tested in the batch liquid phase conversion of *p*-CNB, as a model reactant; the temporal variation of *p*-CNB concentration is shown in Fig. 5(A). We achieved 100% *p*-CAN yield with no evidence of aromatic ring hydrogenation and/or or hydrogenolysis of the –Cl or $–NO_2$ substituents. This ultraselective response, in terms of $–NO_2$ group reduction, is a significant finding when considering the number of studies dealing with liquid phase

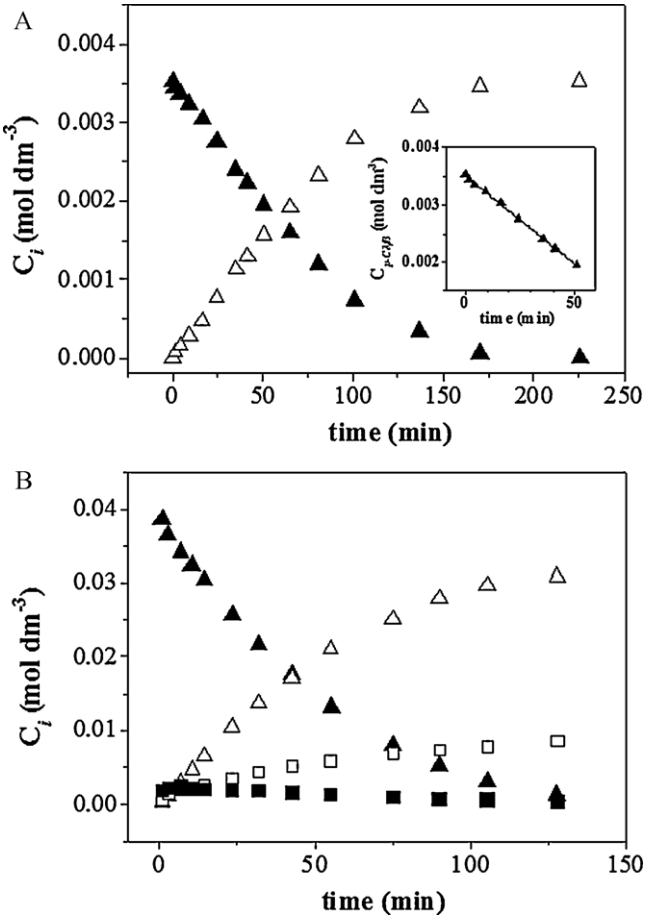

Fig. 5. Temporal variation of *p*-CNB (▲), *p*-CAN (△), NB (■) and AN (□) concentration (C_i) for reaction over (A) β-Mo_2N and (B) Pd/Al_2O_3. Inset to (A): linear fit to temporal $C_{p\text{-CNB}}$ used to obtain initial rate ($R_{p\text{-CNB}}$); P_{H_2} = 11 bar, T = 423 K, *p*-CNB/β-Mo_2N = 0.2 $mol_{p-CNB}\ mol^{-1}_{\beta-Mo_2N}$, *p*-CNB/Pd = 480 $mol_{p\text{-CNB}}\ mol^{-1}_{Pd}$.

catalytic *p*-CNB hydrogenation where C–Cl bond scission has been a feature of reaction over mono- (Ni [4], Pd [64], Pt [65] and Ru [66]) and bi- (Pt–X; X = Cr, Mn, Fe, Co, Ni and Cu [67] and LaNiB [4]) metallic catalysts. The target amine product (*p*-CAN) is a high production volume compound used in the manufacture of a range of pesticides, herbicides, pigments, pharmaceuticals and cosmetics [68]. Catalytic activity was quantified in terms of the initial *p*-CNB hydrogenation rate ($R_{p\text{-CNB}} = 3.1 \times 10^{-5}$ mol dm^{-3} min^{-1}), determined from a linear regression of the temporal *p*-CNB concentration profile (see inset to Fig. 5(A)). In order to fully evaluate the performance of β-Mo_2N, we compared the catalytic response with that of an established hydrogenation catalyst (Pd/Al_2O_3) under the same reaction conditions. Indeed, supported Pd has been extensively used to promote the liquid phase hydrogenation of substituted nitroarenes [12,14,16,69], including *p*-CNB [12,70,71]. The temporal concentration profiles for the conversion of *p*-CNB are shown in Fig. 5(B), where it can be seen that the activity in terms of *p*-CNB consumption was significantly higher for Pd/Al_2O_3. We can link this to the greater hydrogen chemisorption capacity exhibited by Pd/Al_2O_3 (Table 1). However, while the nitride delivered 100% yield to the target *p*-CAN, Pd/Al_2O_3 promoted hydrodechlorination with the formation of NB and subsequent hydrogenation to AN with a 78% yield to *p*-CAN at complete *p*-CNB conversion. As emphasised by Somorjai and Kliewer [72], maximising selectivity to high value products is the critical challenge in 21st century chemical processing. The increasing sustainability demand placed on the chemical sector

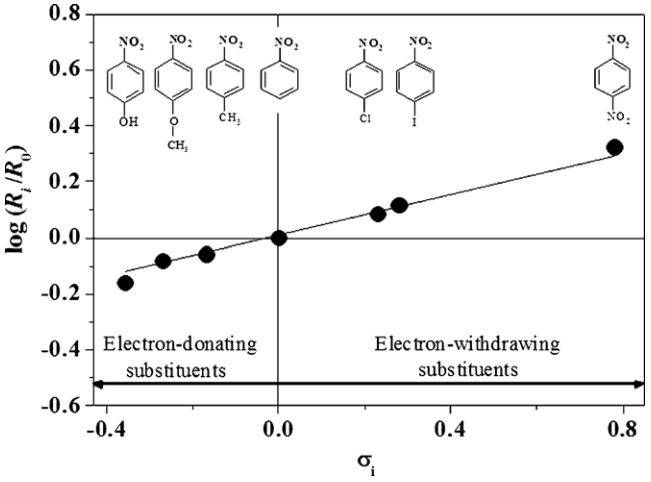

Fig. 6. Hammett plot for the selective –NO_2 group reduction of *para*-substituted nitroarenes over β-Mo_2N at T = 423 K.

is the driver for improved selectivity to avoid costly downstream separations, clean up and disposal. Any step change improvement in catalysis must address crucial selectivity issues. Our results serve to demonstrate the selective catalytic hydrogenation action of β-Mo_2N and the potential for cleaner amine synthesis.

3.2.2. Hydrogenation of para-substituted nitrobenzenes: a Hammett treatment

In order to quantify the effect on reactivity due to the presence of a second functionality in the *para*-position, we investigated the hydrogenation of a series of *para*-substituted (–H, –OH, –O–CH_3, –CH_3, –Cl, –I and –NO_2) nitrobenzenes over β-Mo_2N and applied the Hammett relationship. The Hammett correlation is a practical tool that can be used to predict rate and equilibrium constants [73,74] and elucidate reaction mechanisms [75] without prior experimental determination. In this approach, we relate the initial hydrogenation rate (to the amine) for substituted nitroarene reactants (R_i) to that recorded for the reference benzene derivate (R_0, NB in this case) according to

$$\ln\left[\frac{R_i}{R_0}\right] = \rho \times \sigma_i \quad (5)$$

where σ_i and ρ are the substituent and reaction constants, respectively. The σ_i factor is an empirical parameter that is dependent on the substituent position on the ring and electron donating/acceptor character [76]; reference values are available in the literature [75,76]. The ρ term, or reaction constant, is a measure of the susceptibility of the reaction to substituent electronic effects [77]. When the transition state is negatively charged, the reaction rate is accelerated by electron-withdrawing substituents and $\rho > 0$. Although initially conceived for *non*-catalytic reactions, the applicability of the Hammett approach has been demonstrated for catalyzed homogeneous [74,78,79] and heterogeneous [80,81] processes in both gas [78–80] and liquid [74,81] phase operation. Of direct relevance to this study is the work of Lopidana et al. [82] and Belousov et al. [83] who demonstrated adjustment to the Hammett equation for the liquid phase hydrogenation of polysubstituted nitroarenes over Pt/SiO_2–$AlPO_4$ and Re thiocomplexes, respectively. The applicability of the Hammett relationship to the nitroarene hydrogenation rate data generated using β-Mo_2N is demonstrated in Fig. 6. The slope of the linear fit gives a positive value for ρ (=0.4), which is consistent with a nucleophilic mechanism as proposed elsewhere [84], *i.e.* hydrogen acting as nucleophilic agent that attacks the activated –NO_2 group with the formation of a negatively charged intermediate. The ρ value

obtained in this study is comparable to those reported for the liquid phase hydrogenation of nitro-aromatics over unsupported iron oxide hydroxide [85] and Re thiocomplexes [83] (0.24–0.55) and Pt/SiO_2–$AlPO_4$ (0.1–2.0 [82]) and gas phase operation over Au/TiO_2 (0.93) and Ag/TiO_2 (0.22) [86]. This suggests an analogous reaction mechanism for the formation of amines in these heterogeneous catalysts systems. We provide here, a first insight into the nitroarene hydrogenation mechanism over β-Mo_2N with far ranging implications for processes in the agrochemical, fine chemical and pharmaceutical sectors.

4. Conclusions

β-Mo_2N was synthesized by the temperature programmed treatment (to 933 K) of MoO_3 in N_2/H_2 (15%, v/v) to deliver a crystalline product (BET = 7 $m^2\,g^{-1}$; pore volume = 0.02 $cm^3\,g^{-1}$), characterized by an agglomeration of flake-like structures (1–5 μm). The passivated (in 1%, v/v O_2) nitride exhibited a residual Mo^{6+} content that can be attributed to the superficial oxide layer where XPS analysis indicates a lower Mo oxidation state for β-Mo_2N. Temperature programmed reduction to 637 K was necessary to remove the passivation layer and TPD measurement has revealed a significant quantity of hydrogen (0.7 μmol m^{-2}) associated with the activated β-Mo_2N. The Mo nitride was used as a catalyst in the liquid phase hydrogenation of *p*-CNB where 100% selective with respect to $–NO_2$ group reduction was achieved at complete conversion of the nitroarene. In contrast, Pd/Al_2O_3 (BET area = 157 $m^2\,g^{-1}$, total pore volume = 0.2 $m^3\,g^{-1}$, mean Pd particle size *ca.* 18 nm), used as a benchmark catalyst, was *non*-selective and generated NB and AN (from *p*-CNB) from a combined hydrodechlorination/hydrogenation. The hydrogenation of a range of *para*-substituted (–H, –OH, $–O–CH_3$, $–CH_3$, –Cl, –I and $–NO_2$) nitrobenzenes over β-Mo_2N proceeded *via* a nucleophilic mechanism where the presence of electron withdrawing ring substituents served to elevate rate, as demonstrated by the linear Hammett relationship and positive reaction constant ($\rho = 0.4$). Our results demonstrate the potential of β-Mo_2N to promote the clean production of amino-compounds with multiple industrial applications

Acknowledgements

This work was financially supported by EPSRC (Grant 0231 110525) and the Swiss National Science Foundation. EPSRC support for free access to the TEM/SEM facility at the University of St. Andrews is also acknowledged.

References

[1] P.F. Vogt, J.J. Gerulis, Aromatic amines, in: Ullmann's Encyclopedia of Industrial Chemistry, Wiley-VCH Verlag GmbH & Co. KGaA, Weinheim, 2005.
[2] X.D. Wang, M.H. Liang, J.L. Zhang, Y. Wang, Curr. Org. Chem. 11 (2007) 299.
[3] X. Yan, J. Sun, Y. Wang, J. Yang, J. Mol. Catal. A: Chem. 252 (2006) 17.
[4] Y.-C. Liu, Y.-W. Chen, Ind. Eng. Chem. Res. 45 (2006) 2973.
[5] H. Liu, J. Deng, W. Li, Catal. Lett. 137 (2010) 261.
[6] H.U. Blaser, H. Steiner, M. Studer, ChemCatChem 1 (2009) 210.
[7] M. Mo, L. Han, J. Lv, Y. Zhu, L. Peng, X. Guo, W. Ding, Chem. Commun. 46 (2010) 2268.
[8] H. Li, J. Zhang, H. Li, Catal. Commun. 8 (2007) 2212.
[9] E. Baumgarten, A. Fiebes, A. Stumpe, React. Funct. Polym. 33 (1997) 71.
[10] V. Vishwanathan, V. Jayasri, P.M. Basha, N. Mahata, L.M. Sikhwivhilu, N.J. Coville, Catal. Commun. 9 (2008) 453.
[11] P.M. Reis, B. Royo, Tetrahedron Lett. 50 (2009) 949.
[12] S. Alexander, V. Udayakumar, N. Nagaraju, V. Gayathri, Transit. Met. Chem. 35 (2010) 247.
[13] M. Takasaki, Y. Motoyama, K. Higashi, S.-H. Yoon, I. Mochida, H. Nagashima, Org. Lett. 10 (2008) 1601.
[14] Y. Lang, Q. Wang, J. Xing, B. Zhang, H. Liu, AICHE J. 54 (2008) 2303.
[15] H. Li, Q. Zhao, H. Li, J. Mol. Catal. A: Chem. 285 (2008) 29.
[16] C. Liu, R. Tan, N. Yu, D. Yin, Micropor. Mesopor. Mater. 131 (2010) 162.
[17] B. Zhao, C.-J. Chou, Y.-W. Chen, Ind. Eng. Chem. Res. 49 (2010) 1669.
[18] Y. Li, Y. Fan, J. He, B. Xu, H. Yang, J. Miao, Y. Chen, Chem. Eng. J. 99 (2004) 213.
[19] L. Volpe, M. Boudart, J. Solid State Chem. 59 (1985) 348.
[20] E. Furimsky, Appl. Catal. A: Gen. 240 (2003) 1.
[21] C. Shi, A.M. Zhu, X.F. Yang, C.T. Au, Appl. Catal. A: Gen. 276 (2004) 223.
[22] H. He, H.X. Dai, K.Y. Ngan, C.T. Au, Catal. Lett. 71 (2001) 147.
[23] D. Liu, Y.Q. Liu, T. Zhou, C.G. Liu, G.H. Que, Abstr. Pap. Am. Chem. Soc. 226 (2003) U530.
[24] Z.X. Hao, Z.B. Wei, L.J. Wang, X.H. Li, C. Li, E.Z. Min, Q. Xin, Appl. Catal. A: Gen. 192 (2000) 81.
[25] Z. Wu, Z. Hao, Z. Wei, C. Li, Q. Xin, Stud. Surf. Sci. Catal. 138 (2001) 445.
[26] A. Guerrero-Ruiz, Y. Zhang, B. Bachiller-Baeza, I. Rodríguez-Ramos, Catal. Lett. 55 (1998) 165.
[27] D. Mckay, J.S.J. Hargreaves, J.L. Rico, J.L. Rivera, X.-L. Sun, J. Solid State Chem. 181 (2008) 325.
[28] F. Cárdenas-Lizana, S. Gómez-Quero, N. Perret, L. Kiwi-Minsker, M.A. Keane, Catal. Sci. Technol., in press, doi:10.1039/C0CY00011F.
[29] D.R. Lide, Handbook of Chemistry and Physical Properties, Taylor Francis Group, Boca Raton, USA, 2008.
[30] A.G. Cairns, J.G. Gallagher, J.S.J. Hargreaves, D. McKay, J.L. Rico, K. Wilson, J. Solid State Chem. 183 (2010) 613.
[31] G.M. Maksimova, A.L. Chuvilin, E.A. Moroz, V.A. Likholobov, K.I. Matveev, Kinet. Catal. 45 (2004) 870.
[32] R.J. Madon, M. Boudart, Ind. Eng. Chem. Fundam. 21 (1982) 438.
[33] S. Gong, H. Chen, W. Li, B. Li, Appl. Catal. A: Gen. 279 (2005) 257.
[34] S.W. Gong, H.K. Chen, W. Li, B.Q. Li, Energy Fuels 20 (2006) 1372.
[35] Z. Wei, Q. Xin, P. Grange, B. Delmon, J. Catal. 168 (1997) 176.
[36] C.W. Colling, J.-G. Choi, L.T. Thompson, J. Catal. 160 (1996) 35.
[37] J. Światowska-Mrowiecka, S.d. Diesbach, V. Maurice, S. Zanna, L. Klein, E. Briand, I. Vickridge, P. Marcus, J. Phys. Chem. C 112 (2008) 11050.
[38] Z. Li, L. Gao, S. Zheng, Mater. Lett. 57 (2003) 4605.
[39] D. Mckay, J.S.J. Hargreaves, R.F. Howe, Catal. Lett. 112 (2006) 109.
[40] L. Volpe, S.T. Oyama, M. Boudart, Preparation of Catalysis III, Elsevier, Amsterdam, 1983.
[41] J.-G. Choi, J.R. Brenner, C.W. Colling, B.G. Demczyk, J.L. Dunning, L.T. Thompson, Catal. Today 15 (1992) 201.
[42] J.R. Regalbuto, J.-W. Ha, Catal. Lett. 29 (1994) 189.
[43] P. Ettmayer, Mon. Chem. 101 (1970) 127.
[44] A.G. Cairns, J.G. Gallagher, J.S.J. Hargreaves, D. Mckay, E. Morrison, J.L. Rico, K. Wilson, J. Alloys Compd. 479 (2009) 851.
[45] J.G. Choi, R.L. Curl, L.T. Thompson, J. Catal. 146 (1994) 218.
[46] R.S. Wise, E.J. Markel, J. Catal. 145 (1994) 344.
[47] X.S. Li, Y.X. Chen, Y.J. Zhang, C.X. Ji, Q. Xin, React. Kinet. Catal. Lett. 58 (1996) 391.
[48] M. Saito, R.B. Anderson, J. Catal. 63 (1980) 438.
[49] Y.J. Zhang, Y.X. Li, C. Li, Q. Xin, Adsorption and migration of hydrogen on different surface sites of γ-Mo_2N catalyst, in: Spillover and Migration of Surface Species on Catalysts, Elsevier, Amsterdam, 1997.
[50] A. Guerrero-Ruiz, Q. Xin, Y.J. Zhang, A. Maroto-Valiente, I. Rodriguez-Ramos, Langmuir 15 (1999) 4927.
[51] X.S. Li, Y.J. Zhang, Q. Xin, C.X. Ji, Y.F. Miao, L. Wang, React. Kinet. Catal. Lett. 57 (1996) 177.
[52] J.-G. Choi, H.J. Lee, L.T. Thompson, Appl. Surf. Sci. 78 (1994) 299.
[53] G.W. Haddix, J.A. Reimer, A.T. Bell, J. Catal. 108 (1987) 50.
[54] I. Pettiti, S. Colonna, S.D. Rossi, M. Faticanti, G. Minelli, P. Porta, Phys. Chem. Chem. Phys. 6 (2004) 1350.
[55] E. Elaloui, A.C. Pierre, G.M. Pajonk, J. Catal. 166 (1997) 340.
[56] J.E. Benson, H.S. Hwang, M. Boudart, J. Catal. 30 (1973) 146.
[57] S. Gómez-Quero, F. Cárdenas-Lizana, M.A. Keane, Ind. Eng. Chem. Res. 47 (2008) 6841.
[58] C. Amorim, M.A. Keane, J. Chem. Technol. Biotechnol. 83 (2008) 662.
[59] M. Boudart, H.S. Hwang, J. Catal. 39 (1975) 44.
[60] F. Cárdenas-Lizana, S. Gómez-Quero, M.A. Keane, Appl. Catal. A: Gen. 334 (2008) 199.
[61] M.A. Aramendía, V. Boráu, I.M. García, C. Jiménez, F. Lafont, A. Marinas, J.M. Marinas, F.J. Urbano, J. Catal. 187 (1999) 392.
[62] G.M. Tonetto, D.E. Damiani, J. Mol. Catal. A: Chem. 202 (2003) 289.
[63] T. Janiak, J. Okal, Appl. Catal. B: Environ. 92 (2009) 384.
[64] V. Kratky, M. Kralik, M. Mecarova, M. Stolcova, L. Zalibera, M. Hronec, Appl. Catal. A: Gen. 235 (2002) 225.
[65] X.-X. Han, R.-X. Zhou, G.-H. Lai, X.-M. Zheng, React. Kinet. Catal. Lett. 83 (2004) 55.
[66] Z. Yu, S. Liao, Y. Xu, B. Yang, D. Yu, J. Mol. Catal. A: Chem. 120 (1997) 247.
[67] X.-X. Han, R.-X. Zhou, G.-H. Lai, X.-M. Zheng, Catal. Today 93–95 (2004) 433.
[68] G. Konnecker, A. Boehncke, S. Schmidt, Fresenius Environ. Bull. 12 (2003) 589.
[69] V.L. Khilnani, S.B. Chandalia, Org. Process Res. Dev. 5 (2001) 263.
[70] Q. Xu, X.-M. Liu, J.-R. Chen, R.-X. Li, X.-J. Li, J. Mol. Catal. A: Chem. 260 (2006) 299.
[71] H. Liu, M. Liang, C. Xiao, N. Zheng, X. Feng, Y. Liu, J. Xie, Y. Wang, J. Mol. Catal. A: Chem. 308 (2009) 79.
[72] G.A. Somorjai, C.J. Kliewer, React. Kinet. Catal. Lett. 96 (2009) 191.
[73] L.P. Hammett, J. Am. Chem. Soc. 59 (1937) 96.
[74] M. Alamé, M. Jahjah, S. Pellet-Rostaing, M. Lemaire, V. Meille, C.d. Bellefon, J. Mol. Catal. A: Chem. 271 (2007) 18.
[75] H.H. Jaffé, Chem. Rev. 53 (1953) 191.

[76] C.D. Johnson, The Hammett Equation, Cambridge University Press, Cambridge, 1973.
[77] J. Shorter, Chem. Listy 94 (2000) 210.
[78] T. Kamitanaka, T. Matsuda, T. Harada, Tetrahedron Lett. 44 (2003) 4551.
[79] Y. Himeda, N. Onozawa-Komatsuzaki, H. Sugihara, K. Kasuga, J. Photochem. Photobiol. A: Chem. 182 (2006) 306.
[80] T. Yoneda, T. Takido, K. Konuma, J. Mol. Catal. A: Chem. 265 (2007) 80.
[81] J.R. Ruiz, C. Jiménez-Sanchidrián, J.M. Hidalgo, Catal. Commun. 8 (2007) 1036.
[82] M.A.A. Lopidana, V.B. Bolos, C.J. Sanchidrian, J.M.M. Rubio, F.R. Luque, Bull. Chem. Soc. Jpn. 60 (1987) 3415.
[83] V.M. Belousov, T.A. Palchevskaya, L.V. Bogutskaya, React. Kinet. Catal. Lett. 36 (1988) 369.
[84] B. Coq, F. Figuéras, Coord. Chem. Rev. 178–180 (1998) 1753.
[85] M. Lauwiner, P. Rys, J. Wissmann, Appl. Catal. A: Gen. 172 (1998) 141.
[86] F. Cárdenas-Lizana, Z.M.D. Pedro, S. Gómez-Quero, M.A. Keane, J. Mol. Catal. 326 (2010) 48.